NUMERICAL STUDIES ON PATTERNING OF SHEAR ZONES IN GRANULAR BODIES

JACEK TEJCHMAN

Institute for Concrete Structures,
Technical University of Gdansk,
Narutowicza 11/12, 80-952 Gdansk, Poland
tejchmk@pg.gda.pl

Absteact: The paper deals with numerical investigations on the patterning of shear zones in granular bodies. The behaviour of dry sand during plane strain compression tests was numerically modelled with a finite element method using a hypoplastic constitutive relation within a polar (Cosserat) continuum. The constitutive relation was obtained through an extension of a non-polar one by polar quantities, *viz.* rotations, curvatures, couple stresses using the mean grain diameter as a characteristic length. This relation can reproduce the essential features of granular bodies during shear localisation. The material constants can be easily determined from element test results and can be estimated from granulometric properties. The attention is laid on the influence of boundary conditions and the distribution of imperfections in the granular specimen on the formation of patterns of shear zones.

1. Introduction

Localisation of deformation in the form of narrow zones of intense shearing can develop in granular bodies during processes of granular flow or shift of objects with sharp edges against granular materials. Shear localisation can occur in a single zone, in several zones or in a regular pattern. It can also appear along walls of stiff structures at granular bodies. The determination of the thickness of shear zones is of crucial importance for a realistic estimation of forces transferred from granular bodies to structures, *e.g.* foundations, piles, earth retaining walls or silos (Tejchman 1989, Brinkgreve 1994, Tejchman 1997). Since the shearing resistance can increase with decreasing zone thickness (Tejchman 1998, 2000), resulting dimensionless

forces are scale-dependent. The thickness of a wall shear zone has also an effect on the wall friction angle since both quantities are closely connected (Tejchman 1997). A better understanding of shear zones is also important since they usually signify the failure of granular bodies.

In this paper, shear localisation in the form of a single or several zones was investigated during plane strain compression tests. The FE–analysis was performed with a finite element method on the basis of a hypoplastic law with polar extensions which takes into account the effect of density, pressure, deformation direction and mean grain diameter. During FE–calculations, the emphasis was placed on the influence of conditions along boundaries of the granular specimen and imperfections inside of the specimen. The specimen size was always the same. In addition, the effect of the initial void ratio, pressure level, mean grain diameter and initial stress state on the thickness and the distance of shear zones was studied.

A single shear zone inside of granular bodies was experimentally studied with a biaxial device (Vardoulakis 1980, Yoshida et al. 1994, Tatsuoka et al. 1994, Pradhan 1997), with a simple shear apparatus (Budhu 1984), with an improved direct shear device (Wernick 1978), with a triaxial cell (Roscoe 1970, Lade 1982, Desrues and Hammad 1989, Desrues et al. 1996, Yagi et al. 1997) and with a torsional shear device (Schanz et al. 1997). Several shear zones were observed with a simple shear apparatus (Scarpelli and Wood 1982), a biaxial apparatus (Han and Vardoulakis 1995), with a triaxial cell (Desrues et al. 1996), in model tests with footings (Tatsuoka et al. 1991), during shear tests (Stazhevskii and Revushenko 1992, Tejchman 1997), in earth pressure tests (Schwing 1991, Tejchman 1997), during trap-door experiments (Vardoulakis et al. 1981) and in tests in a hopper (Tejchman 1989). The behaviour of granular bodies along a wall with different roughness was experimentally investaigated with a Casagrande shear apparatus (Potyondy 1961, Sondermann 1983, Desai et al. 1985), with an improved direct shear device (Wernick 1978, Tejchman 1997), with a torsional ring shear apparatus (Neuffer and Leibnitz 1964, Yoshimi and Kishida 1981, Löffelmann 1989), with a ring shear device (Brummund and Leonards 1973), with a simple shear device by Roscoe (Uesugi et al. 1988), with a biaxial apparatus (Tejchman 1989, Tejchman and Wu 1995), with a Couette apparatus (Löffelmann 1989), with model silo tests (Tejchman 1989, Nedderman and Laohakul 1980) and with pull-out tests (Wernick 1978).

Experimental results show that the thickness of a shear zone inside granular bodies is not constant. It increases with increasing grain diameter (Tejchman 1989, Vardoulakis 1980, Yoshida et al. 1994, Hassan 1995), wall stiffness (Löffelmann 1989), wall roughness (Tejchman 1989, Uesugi et al. 1988, Unterreiner et al. 1994, and shear velocity (Löffelmann 1989), and decreases with increasing initial density (Tejchman 1989, Hassan 1995). The influence of grain properties and of the direction of the deformation has not been studied to such an extent (Yoshida et al. 1994). The effect of the pressure level on the thickness of a shear zone has not yet been clarified. Biaxial tests (Desrues and Hammad 1989, Yoshida et al. 1994), showed a decrease of the thickness with increasing pressure. However, wall friction

tests (Löffelmann 1989, Hassan 1995) and silo model tests (Tejchman 1989, Nedderman and Laohakul 1980) performed in the range of low pressures, demonstrated an inverse trend. The observed thickness of shear zones inside of granular bodies varies from 5 to 20 times the mean grain diameter d_{50} (Vardoulakis 1980, Yoshida *et al.* 1994, Desrues and Hammad 1989). It varies from $1 \times d_{50}$ along a smooth wall up to $40 \times d_{50}$ along a very rough wall (Tejchman 1989). The distance between shear zones was found to be dependent on the void ratio of the granular specimen, conditions along the boundaries, sample size and imperfections (Lade 1982, Gudehus 1986, Han and Vardoulakis 1991, Desrues *et al.* 1996, Tejchman 1997). The observed localisation patterns had often a character of self-organisation (Gudehus 1986, Desrues *et al.* 1996, Tejchman 1997). Within shear zones, pronounced grain rotations (Oda *et al.* 1982, Uesugi *et al.* 1988, Tejchman 1989, Löffelmann 1989) and couple stresses (Oda 1993), large strain gradients (Yoshida *et al.* 1994) and high void ratios (Desrues *et al.* 1996, Oda *et al.* 1997) are observed. Tests by Desrues *et al.* 1996 revealed that the void ratio in a shear zone was equal to its critical value. However, Oda *et al.* (1997) and Oda and Kazama (1999) found void ratios in the shear zone higher than critical.

The formation of shear zones inside granular bodies has been numerically investigated within continuum mechanics using different approaches: softening elasto-plastic (Shuttle and Smith 1988, Needleman and Tvergaard 1992, dual-yield hardening elasto-plastic (Ramakrshnan and Atluri 1994, Hicks 1998), hardening elasto-plastic with enriched shape functions (Leroy and Ortiz 1989), hardening elasto-plastic with remeshing (Pastor and Peraire 1989, Hicks 1998), hardening elasto-plastic using an explizit technique (Cundall 1989, Hobbs and Ord 1989, Poliakov *et al.* 1994), hardening and softening elasto-plastic with bifurcation analysis (de Borst 1988), softening visco-plastic (Loret and Prevost 1991, Sluys 1992, Belytschko *et al.* 1994), softening non-local elasto-plastic (Brinkgreve 1994), softening elasto-plastic with higher-order gradients (de Borst *et al.* 1992, Pamin 1994), softening polar elasto-plastic (Mühlhaus 1989, Tejchman 1989, de Borst 1991, Tejchman and Wu 1993, Dietsche 1993, Tejchman 1997), and softening polar hypoplastic (Tejchman and Bauer 1996, Tejchman 1997, Tejchman and Herle 1999, Tejchman *et al.* 1999, Tejchman 2000). FE–results within a conventional continuum were determined by the resolution of the mesh and thus produced unreliable results, *i.e.* the shear zones became narrower upon mesh refinement and computed force-displacement curves were considerably depending on the thickness of the calculated shear zone (Tejchman 1989, 1994, 1997, Brinkgreve 1994). Thus, a realistic modelling of the thickness of shear zones is only possible with constitutive relations which include a characteristic length (Mühlhaus 1989, Tejchman 1989, de Borst *et al.* 1992). FE–results converge to the finite size of the shear zone in a mesh refinement (Mühlhaus 1989, Tejchman 1997) and initial and boundary value problems become mathematically well-posed (Benallal *et al.* 1987, Mühlhaus 1989, de Borst *et al.* 1992). A polar approach seems to be more suitable for regularisation in granular bodies than other models such as non-local, strain gradient and viscous

(Sluys 1992). It takes into account rotations and couple stresses which are observed during shearing but remain negligible during more uniform deformation (Tejchman 1989, Oda *et al.* 1982). Numerical results obtained with a polar hypoplastic law (Tejchman 1998, Tejchman *et al.* 1999, Bauer and Huang 1999, Tejchman 2000) showed that the thickness of a shear zone appearing inside a granular body during biaxial tests and shearing of an infinite planar layer increases with increasing initial void ratio, pressure level and mean grain diameter. The geometry of shear zones and the distance between them was found to be dependent on the distribution of imperfections (Hobbs and Ord 1989, Tejchman and Wu 1993), system size, confining pressure, shear modulus and ratio of wave propagation to velocity of loading (Poliakow *et al.* 1994, Tejchman and Wu 1997).

The paper is organised as follows. At the beginning, a polar hypoplastic constitutive model is briefly outlined (Section 2) mentioning advantages and limitations. Attention is also given to the calibration of the constitutive parameters. Next, the finite element implementation is briefly described (Section 3). Results for plane strain compression tests are presented in Section 4. In Section 5 some conclusions are outlined.

2. Material behaviour

2.1 Hypoplasticity

Hypoplastic constitutive models are an alternative to elasto-plastic formulations for modelling granular materials (Kolymbas 1987, Gudehus 1994, 1996, 1997, 1998, Bauer 1996, von Wollersdorff 1996, Wu *et al.* 1996, Wu and Niemunis 1996, Herle 1997, 1998). In contrast to elasto-plastic models, a decomposition of deformation into elastic and plastic parts is not made. Yield surfaces, plastic potentials, flow rules and hardening and softening rules are not needed. Parameters of recent hypoplastic models are closely related to granulometric properties and can thus be estimated from mean grain diameter, non-uniformity, grain shape and grain hardness (Herle 1997, 1998). They hold for a wide range of densities and pressures.

Hypoplastic models describe the mechanical rearrangement of so-called simple grain skeletons assuming that the macroscopic state can be sufficiently characterised by mean values of stress and density. The following properties are incorporated:

— the state is fully defined through the skeleton (or effective stress) and the void ratio (inherent anisotropy is not considered, and vanishing stresses are not allowed);

— deformation results only from grain rearrangements (small deformations with nearly elastic behaviour of grain contacts are not considered);

— granulometric properties are permanent, *i.e.* abrasion and crushing of grains are restricted;

— there are pressure-dependent minimum, maximum and critical void ratios;

— the material exhibits an asymptotic behaviour for monotonous and cyclic stretching and SOM-states for proportional compression;

— the response is rate-independent;

— physico-chemical effects, in particular capillary and osmotic pressures, and cementation of grain contacts are not taken into account.

The hypoplastic relations are of the rate type and consist of non-linear tensorial functions. Due to the incremental non-linearity with regard to the deformation rate, a hypoplastic model can describe non-linear stress-strain and volumetric behaviour up to and after the peak with a single tensorial equation. Also included is the dependence on pressure level, density and direction of deformation rate, and dilatancy or contractancy during shearing with constant pressure, respectively increase and release of pressure during shearing with constant volume. Advantages of the model are its simplicity and an easy procedure for determination of material constants with standard laboratory experiments (Herle 1997, 1998, Herle and Gudehus 1999). In case of quartz sand, the hypoplastic constitutive law is approximately valid in a pressure range 1 kPa $< -\sigma_{kk}/3 < 1000$ kPa (Herle 1997). Below it, additional capillary forces due to the air humidity and van der Waals forces may become important, and above it, grain crushing. A hypoplastic constitutive law cannot, however, describe realistically shear localisation since it has not a characteristic length. In order to take into account a characteristic length and to describe the kinematics and thickness of shear zones in granulates polar terms were introduced into a hypoplastic constitutive model by Gudehus (1996) and Bauer (1996) by means of a polar (Cosserat) continuum (Mühlhaus 1989, Schäfer 1962).

2.2. Polar continuum

A polar (Cosserat) continuum differs from a non-polar one by additional rotations (Schäfer 1962). For plane strain or axial-symmetry each material point has three degrees of freedom: two translations u_1 and u_2, and one rotation ω^c (Figure 1). ω^c is related with the micro-rotation and is not determined by the displacements as
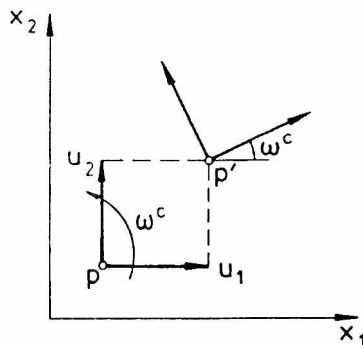

Figure 1. Degrees of freedom in a plane strain Cosserat continuum: u_1 — horizontal displacement, u_2 — vertical displacement, ω^c — Cosserat rotation

in a non-polar continuum:

$$\omega_{ij} = 0.5(u_{i,j} - u_{j,i}). \tag{1}$$

Deformation within a polar continuum is described by the following six quantities (which are considered here as small increments):

$$\varepsilon_{11} = u_{1,1}, \qquad\qquad \varepsilon_{22} = u_{2,2}, \tag{2}$$

$$\varepsilon_{12} = u_{1,2} + \omega^c, \qquad\qquad \varepsilon_{21} = u_{2,1} - \omega^c, \tag{3}$$

$$\kappa_1 = \omega^c_{,1}, \qquad\qquad \kappa_2 = \omega^c_{,2}, \tag{4}$$

ε_{ij} are components of the deformation tensor and κ_i are components of the curvature vector. The extensions are defined similarly as in a non-polar continuum. The deformations ε_{12} and ε_{21} can be viewed as a relative deformation relating the displacement gradient and the micro-rotation; in contrast to a non-polar continuum ε_{12} is not generally equal to ε_{21}. The curvatures κ_1 and κ_2 describe the gradients of the micro-rotation. ε_{ij} and κ_i are invariant with respect to rigid body motions (Mühlhaus 1990). The six deformation quantities are energy-conjugate with the six stress quantities. Four components of ε_{ij} are associated with four components of the stress tensor σ_{ij} which is now in general non-symmetric. The curvatures κ_i are associated with couple stresses m_i. Figure 2 shows stresses σ_{ij} and couple stresses m_i at an element. Force and moment equilibrium require:

$$\sigma_{11,1} + \sigma_{12,2} - f_1^B = 0, \tag{5}$$

$$\sigma_{21,1} + \sigma_{22,2} - f_2^B = 0, \tag{6}$$

$$m_{1,1} + m_{2,2} + \sigma_{21} - \sigma_{12} - m^B = 0, \tag{7}$$

where f_i^B and m^B are the volume body forces and volume body moment, respectively. Equations (5) – (7) are equivalent to the virtual work principle:

$$\int_B (\sigma_{ij}\delta\varepsilon_{ij} + m_i\delta\kappa_i)dV = \int_B (f_i^B\delta u_i + m^B\delta\omega^c)dV + \int_{\partial_1 B} t_i\delta u_i dA + \int_{\partial_2 B} m\delta\omega^c dA. \tag{8}$$

where $t_i = \sigma_{ij}n_j$ and $m = m_i n_i$. t_i and m are prescribed boundary tractions and moment on the boundary $\partial_1 B$ and $\partial_2 B$ with the normal vector n_i, $\delta\varepsilon_{ij}$ and $\delta\kappa_i$ denote virtual deformations and curvatures, respectively, δu_i are virtual displacements, $\delta\omega^c$ is a virtual Cosserat rotation, A stands for the surface, and V denotes the volume. Virtual displacements and Cosserat rotations vanish on those parts of the boundary where kinematic boundary conditions are prescribed. The virtual work principle is used to formulate the FE–equations of motion in a polar continuum (Tejchman 1989, 1997, Sluys 1992, Mühlhaus 1989, Murakami and Yoshida 1997, Groen 1997). As a consequence of micro-rotations and couple stresses, the constitutive equation is endowed with a characteristic length

corresponding to the mean grain diameter. Thus, numerical results become independent of the spatial discretisation, and initial or boundary value problems remain mathematically well-posed. The polar approach can model the thickness of shear zones and scale effects (Mühlhaus 1989, Tejchman 1989, 1997).

An elasto-plastic constituive law within a polar continuum was first proposed by Mühlhaus (1989, 1990), and was successfully applied in various boundary value problems involving shear localisation (Tejchman 1989, 1997, Mühlhaus 1990, Unterreiner *et al.* 1994, de Borst 1991, Tejchman and Wu 1993, 1995 Dietsche 1993, Tejchman and Gudehus 1993, Murakami and Yoshida 1997, Groen 1997, Papanastasiou and Vardoulakis 1992, Steinmann 1995, Yoshida *et al.* 1997).

2.3 Polar hypoplasticity

The polar extension of the hypoplastic law (Tejchman *et al.* 1999, Tejchman and Herle 1999) for the case of plane strain can be abbreviated as:

$$\overset{\circ}{\sigma}_{ij} = F(e, d_{50}, \sigma_{kl}, m_k, d_{kl}^c, k_k). \tag{9}$$

$$\overset{\circ}{m}_i = f(e, d_{50}, \sigma_{kl}, m_k, d_{kl}^c, k_k), \tag{10}$$

σ_{ij} and m_i are the Cauchy stress tensor and Cauchy couple stress vector, respectively, and e denotes the void ratio. The Jaumann stress rate tensor $\overset{\circ}{\sigma}_{ij}$, Jaumann couple stress rate vector $\overset{\circ}{m}_i$, the polar rate of deformation tensor d_{ij}^c and the rate of curvature vector k_i are defined by:

$$\overset{\circ}{\sigma}_{ij} = \dot{\sigma}_{ij} - w_{ik}\sigma_{kj} + \sigma_{ik}w_{kj} \tag{11}$$

$$\overset{\circ}{m}_i = \dot{m}_i - 0.5 w_{ik} m_k + 0.5 m_k w_{ki}, \tag{12}$$

$$d_{ij}^c = d_{ij} + w_{ij} - w_{ij}^c, \quad k_i = w_{,i}^c, \quad w_{kk}^c = 0, \quad w_{21}^c = -w_{12}^c = w^c, \tag{13}$$

$$d_{ij} = 0.5(v_{i,j} + v_{j,i}) \quad w_{ij} = 0.5(v_{i,j} + v_{j,i}), \tag{14}$$

d_{ij} is the classical (non-polar) rate of deformation, w_{ij} denotes the classical (non-polar) spin tensor, $w_c = \dot{\omega}^c$ is the rate of the Cosserat rotation, and v represents the spatial gradient of velocity. If the volume of grains remains constant, the rate of the void ratio can be expressed by:

$$\dot{e} = (1 + e) d_{kk}. \tag{15}$$

The following representations of the constitutive equations are used:

$$\overset{\circ}{\sigma}_{ij} = f_s \left[L_{ij}\left(\hat{\sigma}_{kl}, \hat{m}_k, d_{kl}^c, k_k d_{50}\right) + f_d N_{ij}(\hat{\sigma}_{ij})\sqrt{d_{kl}^c d_{kl}^c + k_k k_k d_{50}^2}\ , \tag{16}$$

$$\overset{\circ}{m}_i / d_{50} = f_s [L_i^c(\hat{\sigma}_{kl}, \hat{m}_k, d_{kl}^c, k_k d_{50}) + f_d N_i^c(\hat{m}_i)\sqrt{d_{kl}^c d_{kl}^c + k_k k_k d_{50}^2}\ , \tag{17}$$

wherein the normalised stress tensor and the normalised couple stress vector are defined by:

$$\hat{\sigma}_{ij} = \frac{\sigma_{ij}}{\sigma_{kk}}, \qquad \hat{m}_i = \frac{m_i}{\sigma_{kk} d_{50}} \; . \tag{18}$$

The scalar factors $f_s = f_s(e, \sigma_{kk})$ and $f_d = f_d(e, \sigma_{kk})$ take into account the influence of the density and pressure level on the stress and the couple stress rates. The stiffness factor f_s is proportional to the granulate hardness h_s and depends on the mean stress and void ratio:

$$f_s = \frac{h_s}{nh_i} \left(\frac{1+e_i}{e} \right) \left(-\frac{\sigma_{kk}}{h_s} \right)^{1-n} , \tag{19}$$

with

$$h_i = \frac{1}{c_1^2} + \frac{1}{3} - \left(\frac{e_{i0} - e_{d0}}{e_{c0} - e_{d0}} \right)^\alpha \frac{1}{c_1\sqrt{3}} \; . \tag{20}$$

The granulate hardness h_s is related to the skeleton. The density factor f_d, kind of a pressure-dependent relative density index, is represented by:

$$f_d = \left(\frac{e - e_d}{e_c - e_d} \right)^\alpha . \tag{21}$$

Here e is the current void ratio, e_c is the critical void ratio, e_d denotes the void ratio at maximum densification due to cyclic shearing, e_i is the maximum void ratio, and α and n are constants. The void ratio e is bounded thus by e_i and e_d. The values of e_i, e_d and e_c are assumed to decrease with the pressure $-\sigma_{kk}$ according to the equations (Bauer 1996)

$$e_i = e_{i0} \exp\left[-\left(-\sigma_{kk}/h_s \right)^n \right], \tag{22}$$

$$e_d = e_{d0} \exp\left[-\left(-\sigma_{kk}/h_s \right)^n \right], \tag{23}$$

$$e_c = e_{c0} \exp\left[-\left(-\sigma_{kk}/h_s \right)^n \right], \tag{24}$$

wherein e_{i0}, e_{d0} and e_{c0} are the values of e_i, e_d and e_c for $\sigma_{kk} = 0$, respectively. For the tensor and vector functions L_{ij}, L_i^c, N_{ij} and N_i^c, the following representations are used:

$$L_{ij} = a_1^2 d_{ij}^c + \hat{\sigma}_{ij}(\hat{\sigma}_{kl}d_{kl}^c + \hat{m}_k k_k d_{50}), \quad L_i^c = a_1^2 k_i d_{50} + a_1^2 \hat{m}_i(\hat{\sigma}_{kl}d_{kl}^c + \hat{m}_k k_k d_{50}), \tag{25}$$

$$N_{ij} = a_1(\hat{\sigma}_{ij} + \hat{\sigma}_{ij}^*), \qquad N_i^c = a_1^2 a_c \hat{m}_i, \tag{26}$$

where:

$$a_1^{-1} = c_1 + c_2 \sqrt{\hat{\sigma}_{kl}^* \hat{\sigma}_{lk}^*} \left[1 + \cos(3\theta) \right], \quad \cos(3\theta) = -\frac{\sqrt{6}}{\left[\hat{\sigma}_{kl}^* \hat{\sigma}_{lk}^* \right]^{1.5}} \left(\hat{\sigma}_{kl}^* \hat{\sigma}_{lm}^* \hat{\sigma}_{mk}^* \right), \quad (27)$$

$$c_1 = \sqrt{\frac{3}{8}} \frac{(3 - \sin\phi_c)}{\sin\phi_c}, \qquad c_2 = \frac{3}{8} \frac{(3 + \sin\phi_c)}{\sin\phi_c}. \tag{28}$$

ϕ_c is the critical angle of internal friction, θ denotes the Lode angle, *i.e.* the angle on the deviatoric plane $\sigma_1 + \sigma_2 + \sigma_3 = 0$ between the stress vector and the axis σ_3 (σ_1 is a principal stress component). The coefficient a_1^{-1} lies empirically in the range 3 to 4.5. The dimensionless polar constant a_c controls the influence of the Cosserat quantities on the material behaviour. It lies in the range of 1.0–5.0 and is correlated with the grain roughness; the higher the constant a_c, the smaller are the polar effects. σ_{ij}^* denotes the deviatoric part of σ_{ij}. For an isotropic stress state with $\hat{\sigma}^* = 0$, $\cos(3\theta) = 0$ and $a_1^{-1} = c_1$ hold in Equation (27).

The polar extension of the hypoplastic law was achieved analogously to Mühlhaus's formulation (1989). First, the term in the non-polar function L_{ij} with the power of the stress ratio tensors and the non-polar modulus of the deformation rate $\|d_{kl}\|$ were extended by the polar quantities $m_k k_k d_{50}$ and $k_k k_k d_{50}^2$, respectively. Therein, the polar deformation rates d_{ij}^c were used. The non-polar function N_{ij} was left unchanged. The polar function L_i^c was similarly defined as L_{ij}. However, the function N_i^c had to be assumed in another way than N_{ij} since the evolution of couple stresses during shearing is different from that of stresses due to their skew symmetry and lack of sign restriction (Tejchman 1994). Assuming that the material has an asymptotic behaviour both for stresses and couple stresses during monotonous shearing, the function N_i^c was found by fitting the numerical results for shearing of an infinite layer between two very rough walls (Tejchman 1994, 1997, 2000) with a theoretical solution within a polar elastic continuum (Schäfer 1962), and with a numerical solution within a polar elasto-plastic continuum (Tejchman 1997). The linear term $f_s L_i^c$ in Equation (17) causes an increase of couple stresses, and the non-linear term $f_s f_d N_i^c \sqrt{d_{kl}^c d_{kl}^c + k_k k_k d_{50}^2}$ in Equation (17) reduces them to reach a stationary value during stationary shearing. Other linear and non-linear representations of N_i^c were tested in FE–calculations. However, the most realistic results were obtained with the given representation of N_i^c. In addition, the function N_i^c in the polar hypoplastic law was verified by results of other boundary value problems involving shear localisation (Tejchman 1997). If the characteristic length d_{50} becomes infinitely small, the polar hypoplastic model (Equations (9) – (28)) reduces to the non-polar one.

The polar hypoplastic constitutive relation includes only 9 constants: e_{i0}, e_{d0}, e_{c0}, ϕ_c, h_s, a, n, d_{50} and a_c. The parameters h_s and n can be determined from a single

J. Tejchman

oedometric compression test with an initially loose specimen; h_s reflects the slope of the curve in a semilogarithmic representation, and n its curvature. The constant a can be found from a triaxial test with a dense specimen. It reflects the height and position of the peak value a the stress-strain curve. ϕ_c is the angle of internal friction in the critical (residual) state which can be estimated from the angle of repose if cohesive forces are negligible or measured in a triaxial test with a loose specimen. It depends mainly on the grain size and angularity, being only little affected by non-uniformity of the grain size distribution (Herle 1997). The values of e_{i0}, e_{d0}, e_{c0} and d_{50} can be obtained with simple index tests ($e_{c0} \approx e_{max}$, $e_{d0} \approx e_{min}$, $e_{i0} \approx 1.5 e_{max}$). All parameters are closely related to the grain size distribution and grain shape as was shown by Herle and Gudehus (1999), and Herle (1997) for various quartz sands. The following material constants for so-called Karlsruhe sand were used: $e_{i0} = 1.3$, $e_{d0} = 0.51$, $e_{c0} = 0.82$, $\phi_c = 30°$, $h_s = 190$ MPa, $a = 0.3$, $n = 0.5$, $d_{50} = 0.5$ mm. The polar constant was found to be $a_c = a_1^{-1}$.

The capability of a polar hypoplastic approach in solving boundary value problems involving localisation such as biaxial test, simple shearing, silo flow, footing, sand anchor was demonstrated by Tejchman *et al.* (1999), Tejchman and Bauer (1996), Tejchman (1997), Tejchman and Herle (1998, 1999), Wehr *et al.* (1998), Wehr and Tejchman (1999). A close agreement between calculations and experiments was achieved. The FE–calculations showed also that the thickness of shear zones did not depend upon the mesh discretisation if the size of finite elements in the shear zone was not more than five times the mean grain diameter when using triangular finite elements with linear shape functions for displacements and a Cosserat rotation (Tejchman and Bauer 1996, Tejchman 1997). Numerical calculations by Sluys (1992) and Groen (1997) within a polar continuum also indicate that convergence to a unique solution can only be obtained when the element size is small enough compared to the width of the localised zone.

3. Finite Element implementation

The FE–calculations of quasi-static plane strain compression tests were performed for a sand specimen with a height of $h = 50$ mm and a length of $l = 100$ mm. Quadrilateral finite elements composed of four diagonally crossed triangles were applied to avoid volumetric locking (Nagtegaal *et al.* 1974, Groen 1997). Totally, 3200 triangular elements were used. The height and the width of the quadrilateral elements was 2.5 mm ($5 \times d_{50}$). The integration was performed with three sampling points placed in the middle of each element side. Linear shape functions for displacements and the Cosserat rotation were used. The calculations were carried out with large deformations and curvatures (updated Lagrange formulation), changing the element configuration and the element volume (Bathe 1982). As the initial stress state in the granular specimen, a K_0–state without polar quantities ($\sigma_{22} = \gamma_d x_2$, $\sigma_{11} = \sigma_{33} = K_0 \gamma_d x_2$, $\sigma_{12} = \sigma_{21} = m_1 = m_2 = 0$) was assumed ($\sigma_{11}$ – horizontal normal stress, σ_{22} – vertical normal stress, σ_{12} – horizontal shear stress, σ_{21} – vertical shear stress, m_1 – horizontal couple stress, m_2 – vertical couple

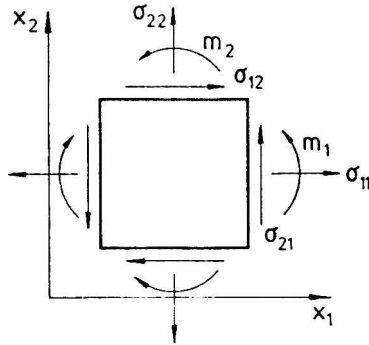**Figure 2.** *Stresses σ_{ij} and couple stresses m_i at an element of a plane strain Cosserat continuum*
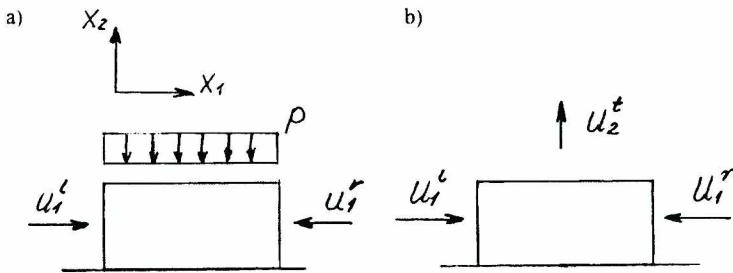

Figure 3. *Plane strain compression test: a) deformation produced by horizontal displacements of both sides ($u_1^l = u_1^r$) and vertical pressure on the top p, b) deformation produced by horizontal displacement of both sides ($u_1^l = u_1^r$), and vertical displacement of the top ($u_1^l = u_1^l = u_1^r$) l — left, r — right, t — top*

stress (Figure 2), γ_d – initial density, x_2 – vertical coordinate measured from the top, $K_0 = 0.4$ – pressure coefficient at rest). In addition, the calculations were carried out with $K_0 = 1.0$.

Two different sets of boundary conditions were assumed. In the first case, the bottom was smooth, the smooth top was subject to the uniform vertical pressure p, and the vertical smooth sides were subject to equal horizontal displacement increments directed to the specimen inside (Figure 3a). The boundary conditions were along the bottom: $u_2 = 0$, $\sigma_{12} = 0$ and $m_1 = 0$, along the top: $\sigma_{22} = -p$, $\sigma_{12} = 0$ and $m_1 = 0$, along the left side: $u_1 = n\Delta u$, $\sigma_{21} = 0$ and $m_2 = 0$, and along the right side: $u_1 = -n\Delta u$, $\sigma_{21} = 0$ and $m_2 = 0$. In the second case, the bottom was smooth, the smooth top was subject to uniform vertical displacement increments directed to the specimen outside, and the vertical smooth sides were subject to equal horizontal displacement increments directed to the specimen inside (Figure 3b). The vertical displacement was equal to the horizontal one. The boundary conditions were along the bottom: $u_2 = 0$, $\sigma_{12} = 0$ and $m_1 = 0$, along the top: $u_2 = n\Delta u$, $\sigma_{12} = 0$ and $m_1 = 0$, along the left side: $u_1 = n\Delta u$, $\sigma_{21} = 0$ and $m_2 = 0$, and along the right side: $u_1 = -n\Delta u$,

$\sigma_{21} = 0$ and $m_2 = 0$. n denotes the number of the time steps, Δu is the constant displacement increment in one step. The displacement increments were chosen as $\Delta u/h = 0.0001$. About 2000 steps were performed.

To produce shear localisation, two different kinds of imperfections were applied. First, a weak element with a large initial void ratio, $e_0 = 0.90$, was inserted in the middle of the left side of the specimen. Second, the initial void ratio was distributed stochastically in the specimen elements by means of a random generator in such a way that the initial void ratio e_0 was increased in every element by the value $a \cdot r$, where $a = 0.05$ and r is a random number within the range of (0.01, 0.99). In addition, the weak element was inserted in the middle of the specimen.

For the solution of the non-linear equation system, a modified Newton-Raphson scheme with line search (Bathe 1982) was used with a global stiffness matrix calculated with only two first terms of the constitutive equations which are linear in
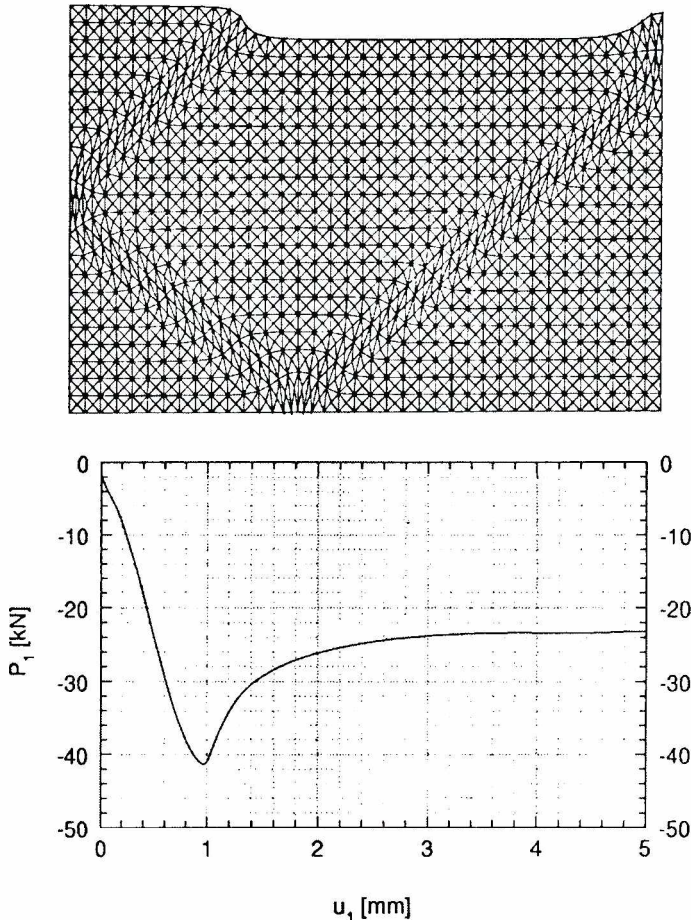
Figure 4. *Deformed mesh at residual state and the evolution of the horizontal force P_1 versus the horizontal displacement u_1 for dense sand ($e_0 = 0.60$, $p = 100$ kPa, $d_{50} = 0.5$ mm)*

d_{kl}^c and kd_{50}. The stiffness matrix was updated every 100–200 steps. To accelerate the calculations in the softening regime, the initial increments of displacements and the Cosserat rotation in each calculation step were assumed to be equal to the entire increments in the previous step (Vermeer and van Langen 1989, Tejchman 1989). The iteration steps were performed using translational and rotational convergence criteria. For the time integration of stresses and couple stresses in finite elements, a one-step Euler forward scheme was applied.

4. Numerical results

The FE–calculations of a plane strain compression test with the boundary conditions of Figure 3a, the K_0-initial stress state ($K_0 = 0.4$) and one weak element in the middle of the left side are shown in Figures 4–9. Figures 4 and 5 show the evolution of the resultant horizontal force acting on the sides with the horizontal
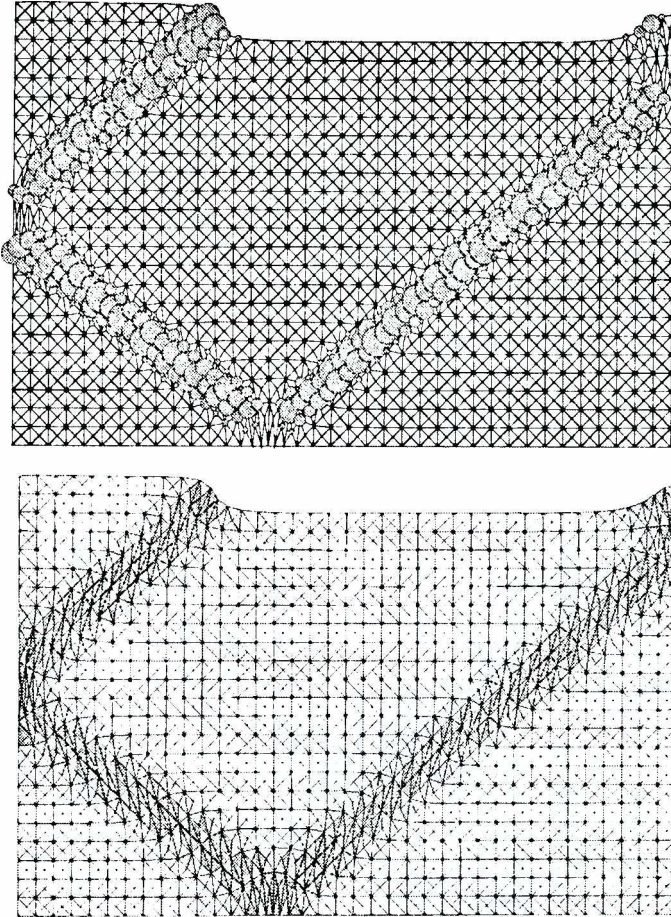
Figure 5. *Distribution of the Cosserat rotation and void ratio for dense specimen*
($e_0 = 0.60$, $p = 100$ kPa, $d_{50} = 0.5$ mm) at residual state ($u_1/h = 0.1$)
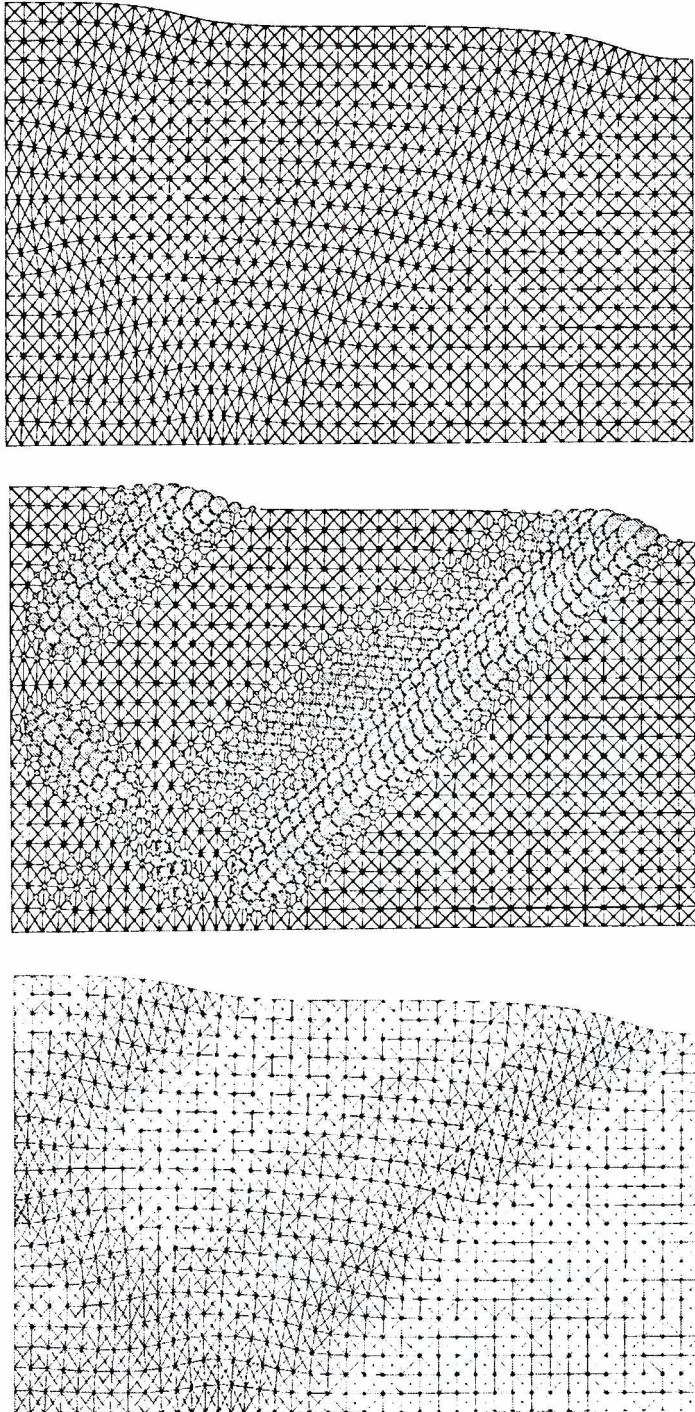
Figure 6. *Deformed mesh and the distribution of the Cosserat rotation and void ratio for medium dense specimen ($e_0 = 0.75$, $p = 100$ kPa, $d_{50} = 0.5$ mm) at residual state ($u_1/h = 0.1$)*
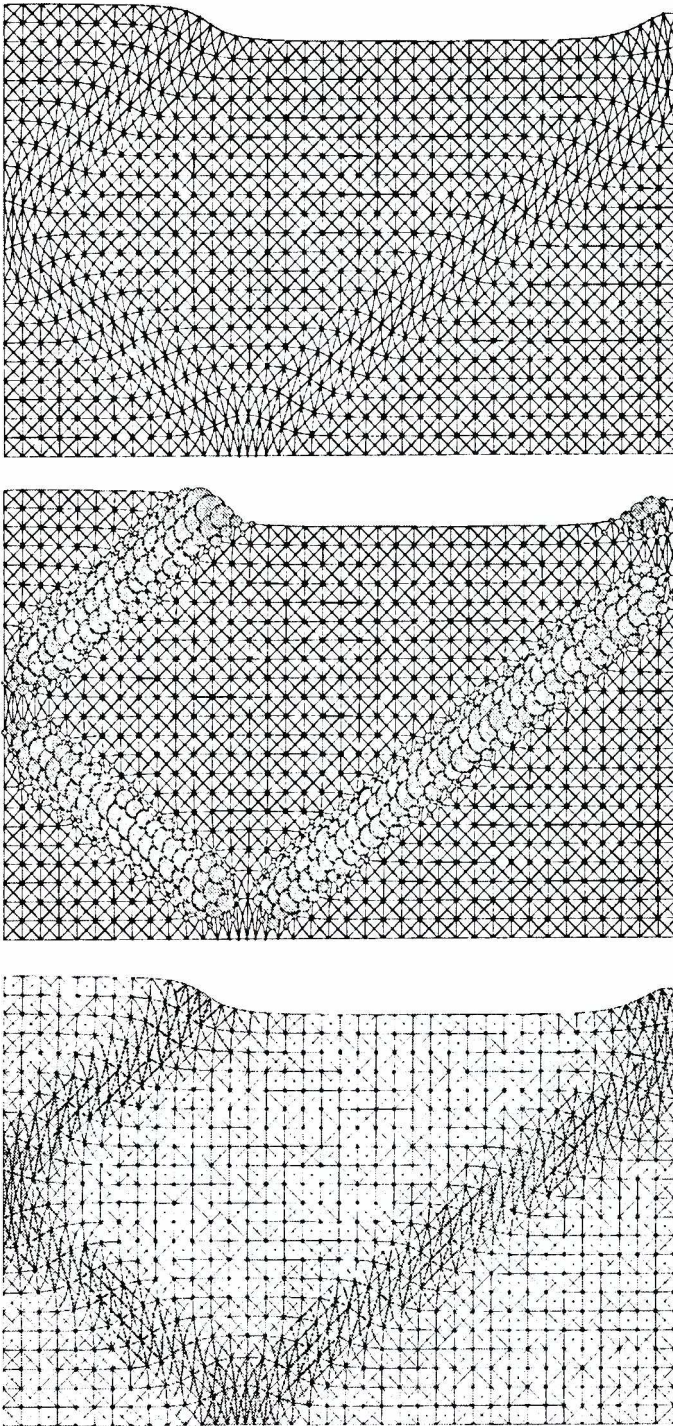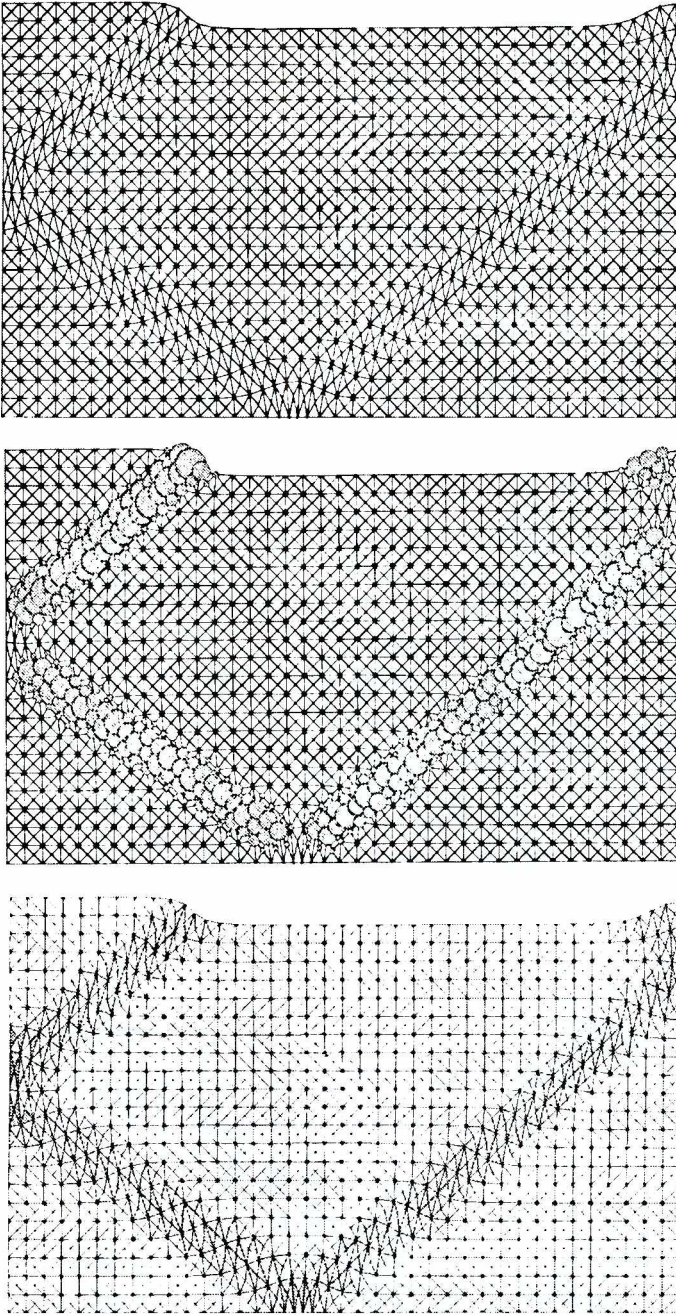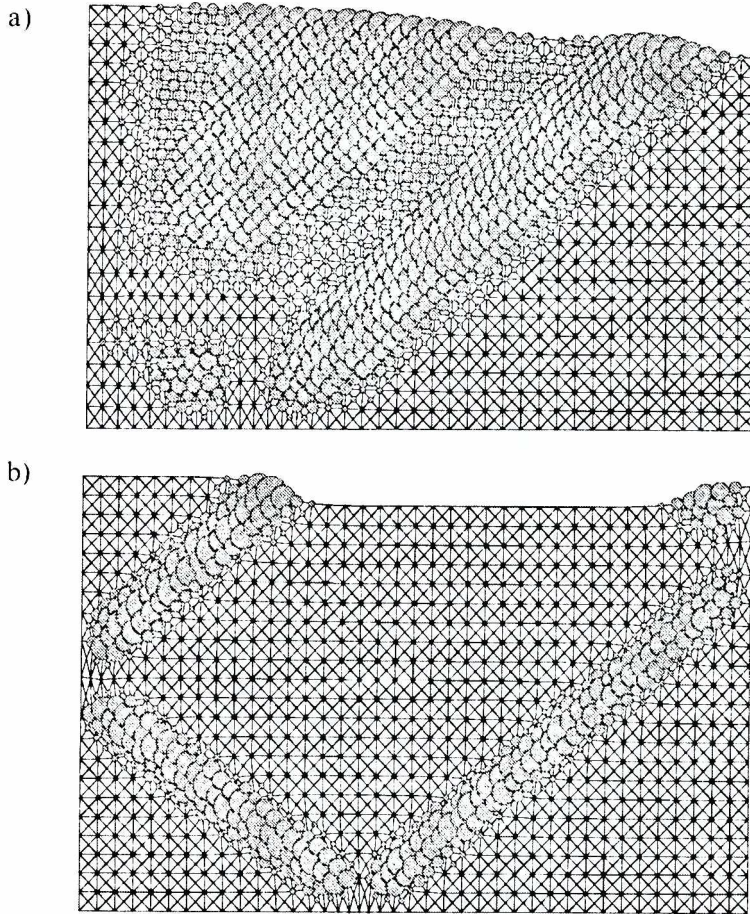
Figure 7. *Deformed mesh and the distribution of the Cosserat rotation and void ratio for dense specimen ($e_0 = 0.60$, $p = 100$ kPa, $d_{50} = 1.0$ mm) at residual state ($u_1/h = 0.1$)*

Figure 8. *Deformed mesh and the distribution of the Cosserat rotation and void ratio for dense specimen ($e_0 = 0.60$, $p = 1000$ kPa, $d_{50} = 0.5$ mm) at residual state ($u_1/h = 0.1$)*

a)

b)

Figure 9. *Distribution of the Cosserat rotation at residual state ($u_t/h = 0.1$): a) loose sand ($e_o = 0.85$, $p = 100$ kPa, $d_{50} = 0.5$ mm, b) dense sand ($e_o = 0.60$, $p = 0$-1000 kPa, $d_{50} = 0.5$ mm)*
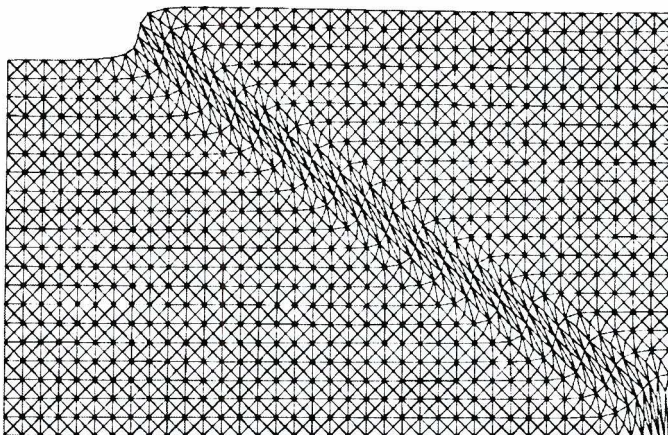
Figure 10. *Deformed mesh for dense sand ($e_o = 0.60$, $p = 100$ kPa, $d_{50} = 0.5$ mm) at residual state ($u_t/h = 0.1$) with one imperfection element in the middle of the specimen*
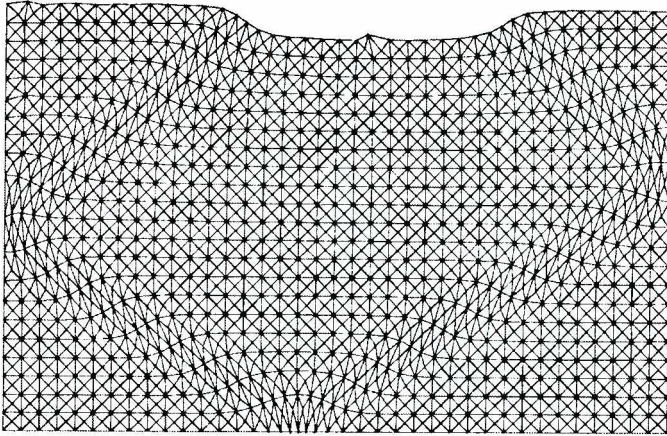
Figure 11. Deformed mesh for dense sand ($e_0 = 0.60$, $p = 100$ kPa, $d_{50} = 0.5$ mm) at residual state ($u_1/h = 0.1$) with $K_0 = 1.0$
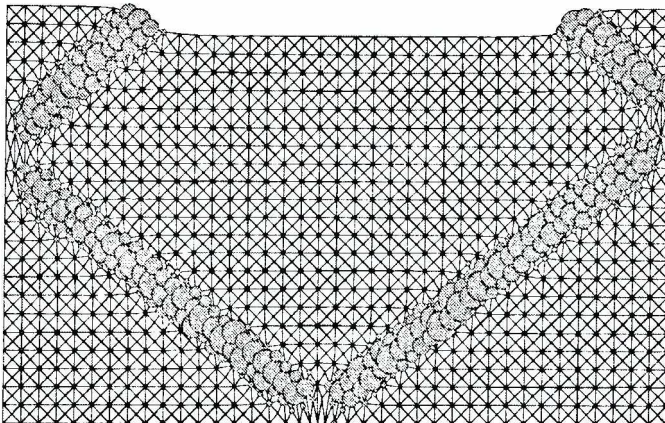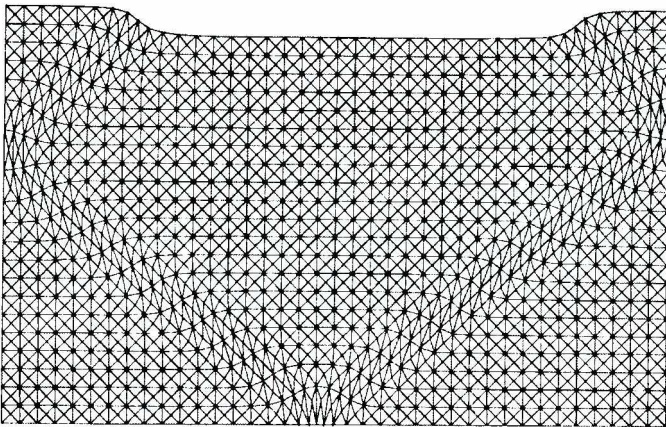

Figure 12. Deformed mesh and the distribution of the Cosserat rotation for dense specimen ($e_0 = 0.60 + 0.05r$; $p = 10$ kPa, $d_{50} = 0.5$ mm) at residual state

Figure 13. Deformed mesh and the distribution of the Cosserat rotation for dense specimen
($e_0 = 0.60 + 0.05r$, $p = 100$ kPa, $d_{50} = 0.5$ mm) at residual state
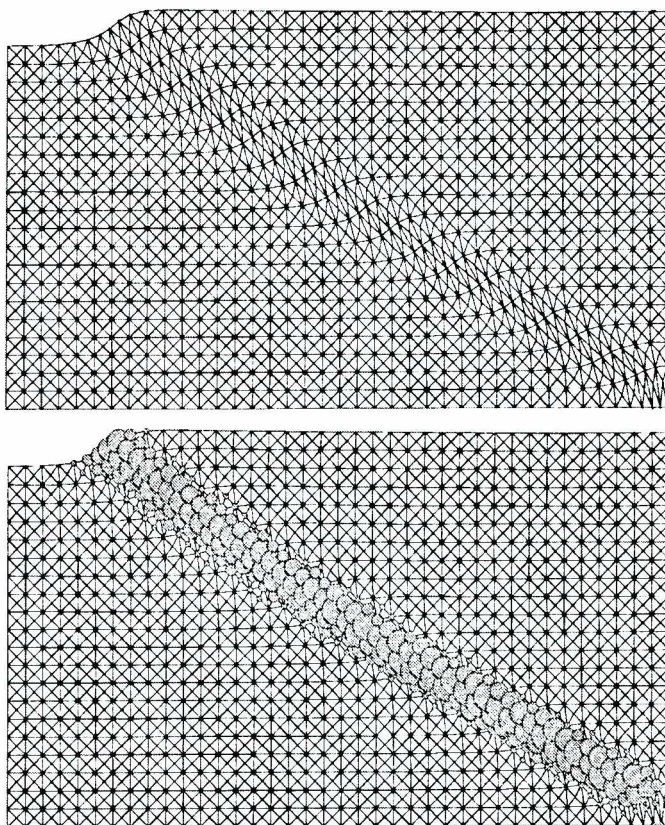
displacement, the deformed FE–mesh, the distribution of the Cosserat rotation and void ratio at residual state for dense sand ($e_0 = 0.60$, $d_{50} = 0.5$ mm, $p = 100$ kPa). The magnitude of the Cosserat rotation is marked by circles with a maximum diameter corresponding to the maximum rotation in the given step. In turn, the grade of an increase of the void ratio is marked by a dark region. Darker region indicates higher void ratio. The void ratios were taken as the mean values in each quadrilateral element.

All state variables (forces, stresses, couple stresses, void ratios) tend to asymptotic values. Due to the formation of shear zones, the calculated horizontal force indicates large softening. The vertical force on the top is constant, and equal to 10 kN. During deformation, two shear zones are first created expanding outward from the weakest element. Afterwards, the shear zone propagating towards the inmovable bottom, reflects from it and moves next to the right side and reflect again towards the top. Thus, four shear zones are visible. The shear zones are marked out
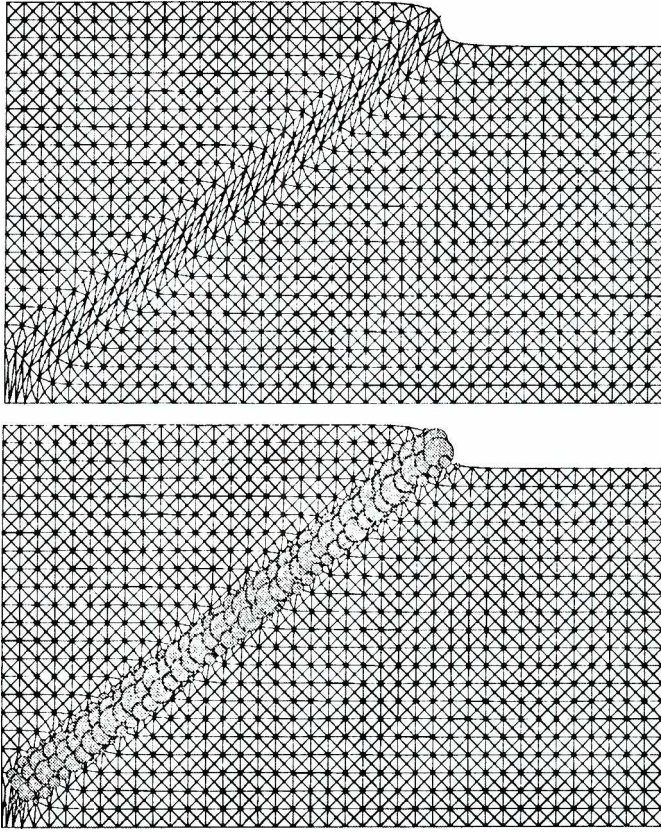
Figure 14. *Deformed mesh and the distribution of the Cosserat rotation for dense specimen*
($e_0 = 0.60 + 0.05r$, $p = 1000$ kPa, $d_{50} = 0.5$ mm) *at residual state*

by the concentration of displacements and Cosserat rotations and by an increase of
the void ratio. The thickness of the shear zones on the basis of displacements and
Cosserat rotations is about $t = 13 \times d_{50}$, and the distance between two inclined shear
zones $s = 90 \times d_{50}$. The thickness of the shear zones on the basis of an increase of
the void ratio is larger since dense granular material dilates before the shear zone is
created (Herle 1997). The Cosserat rotations are only noticeable in the shear zone.
They appear only when a shear zone occurs. Outside the shear zone, they are
negligible. The void ratio changes across the shear zone from 0.65–0.79. Outside the
shear zone, the void ratio is $e = 0.55$, and is lower than its initial value of 0.60 since
the granular material undergoes contractancy at the beginning of shearing.
The largest void ratio in the shear zone corresponds approximately to the critical
value e_c (Equation (24)).

The effect of the initial void ratio e_0, vertical pressure p and the mean grain
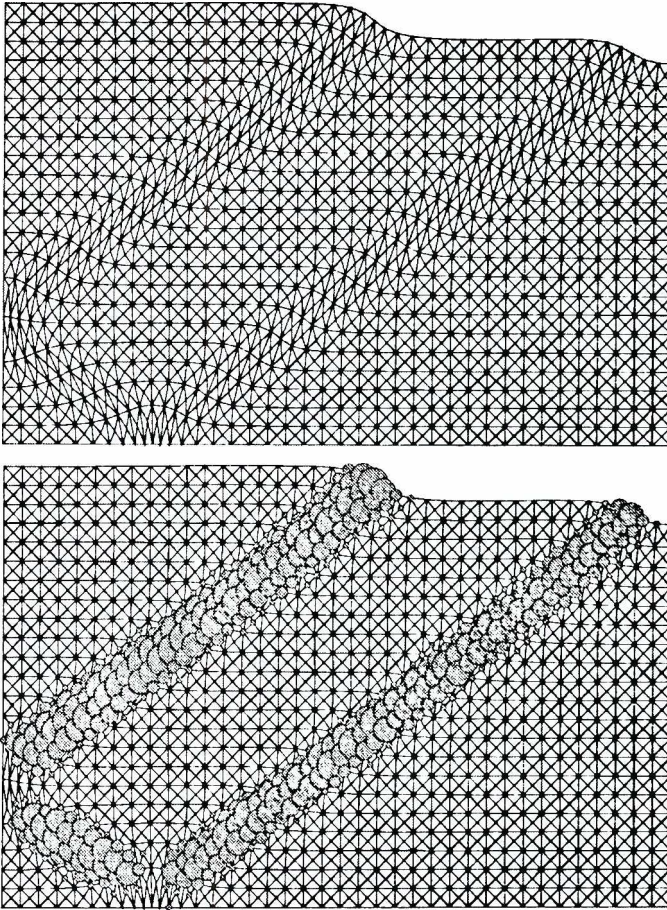diameter d_{50} is presented in Figures 6–8. The following results of t and s were

Figure 15. *Deformed mesh and the distribution of the Cosserat rotation for dense specimen*
$(e_n = 0.60 + 0.05r, \ p = 0 - 100 \ kPa, \ d_{50} = 0.5 \ mm)$ *at residual state*

obtained: $t = 25 \times d_{50}$ and $s = 85 \times d_{50}$ $(e_0 = 0.75, \ d_{50} = 0.5$ mm, $p = 100$ kPa), $t = 9 \times d_{50}$ and $s = 45 \times d_{50}$ $(e_0 = 0.60, \ d_{50} = 1.0$ mm, $p = 100$ kPa), and $t = 15 \times d_{50}$ and $s = 100 \times d_{50}$ $(e_0 = 0.60, \ d_{50} = 0.5$ mm, $p = 1000$ kPa). The results show that the thickness of shear zones increases with increasing initial void ratio, mean grain diameter and vertical pressure. The distance between the inclined zones decreases with increasing e_0 and decreasing p. For $e_0 > e_c$ the thickness of shear zones almost reaches the size of the granular body (Figure 9a). If the linearly increasing vertical pressure (changing from 0 kPa to 1000 kPa) is prescribed (Figure 9b), the increase of the thickness of shear zones with increasing pressure is more pronounced. However, the distance between shear zones remains unchanged. The increase of the mean grain diameter increases the shear zone thickness as a polar granular body
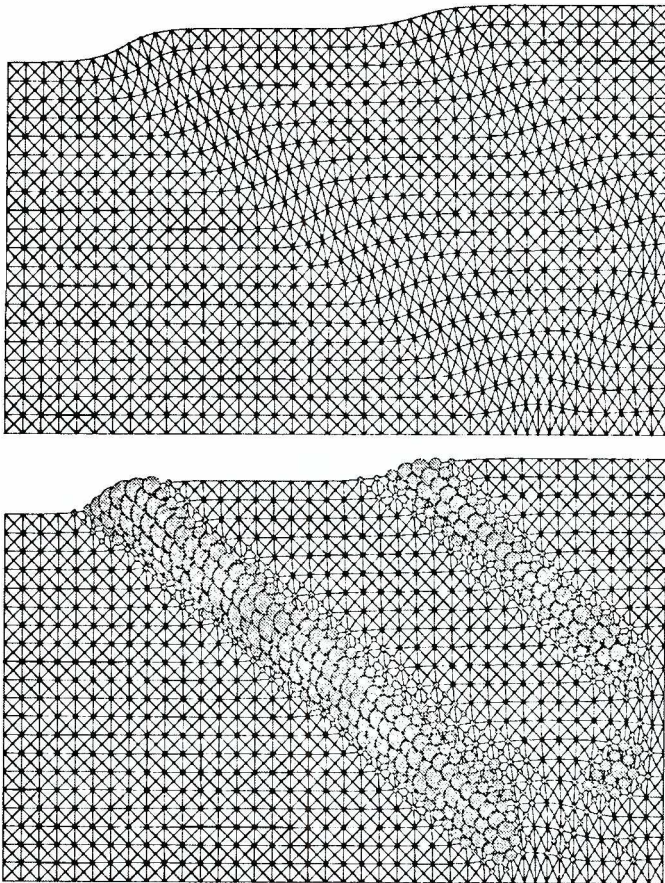
Figure 16. *Deformed mesh and the distribution of the Cosserat rotation for dense specimen*
$(e_0 = 0.70 + 0.05r, \quad p = 100 \ kPa, \ d_{50} = 0.5 \ mm)$ *at residual state*

is stiffer than a non-polar one using the same constants: the stiffness increases with increasing mean grain diameter. The work of a polar continuum (Equation (8)) is augmented, namely, by couple stresses, curvatures and Cosserat rotations which depend upon d_{50}. Thus, the additional degree of freedom of a polar continuum mobilises an additional resistance due to the presence of couple stresses (this corresponds to the stiffness increase of a hinge joint of a frame by prescribing an moment).

The location of the weak element influences the geometry of shear zones. Assuming one weak element in the middle of the specimen, only one shear zone is observed (Figure 10).

The initial stress state has also a effect on the geometry of shear zones (Figure 11). The FE–calculations were carried out with the K_0-initial stress state but with
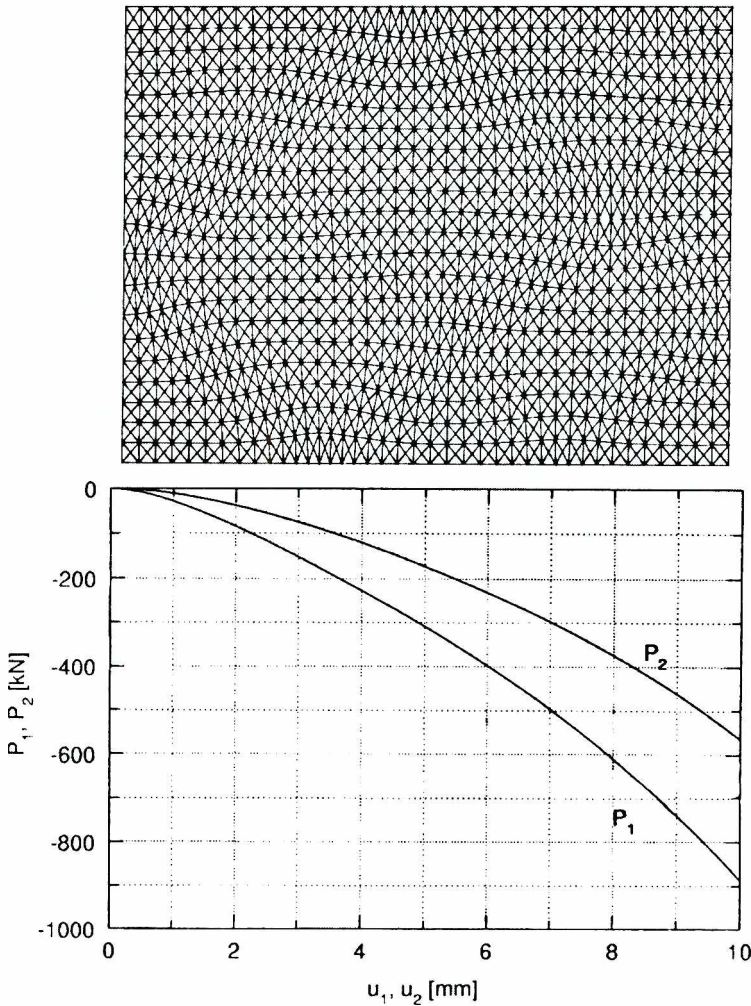
Figure 17. *Deformed mesh at residual state ($u_1/h = 0.2$) and the evolution of the horizontal force P_1 and vertical force P_2 versus the horizontal u_1 and vertical displacement u_2 for dense sand ($e_0 = 0.60 + 0.05r$, $d_{50} = 0.5$ mm)*

$K_0 = 1.0$. In this case, the same quantity of shear zones is created, but the distance between the inclined shear zones is slightly larger ($s = 100 \times d_{50}$).

The numerical results with the boundary conditions of Figure 3a, the K_0-initial stress state ($K_0 = 0.4$) and the stochastic distribution of the initial void ratio in the specimen are shown in Figures 12–16. In the calculations, the vertical pressure and the initial void ratio were varied. The results show that the geometry of shear localisation is strongly influenced by e_0 i p. For the small vertical pressure $p = 10$ kPa (Figure 12), the number of shear zones (4) is similar as in the case with one weak element (Figures 4 and 5). Their thickness ($t = 10 \times d_{50}$) is slightly smaller. However, the distance
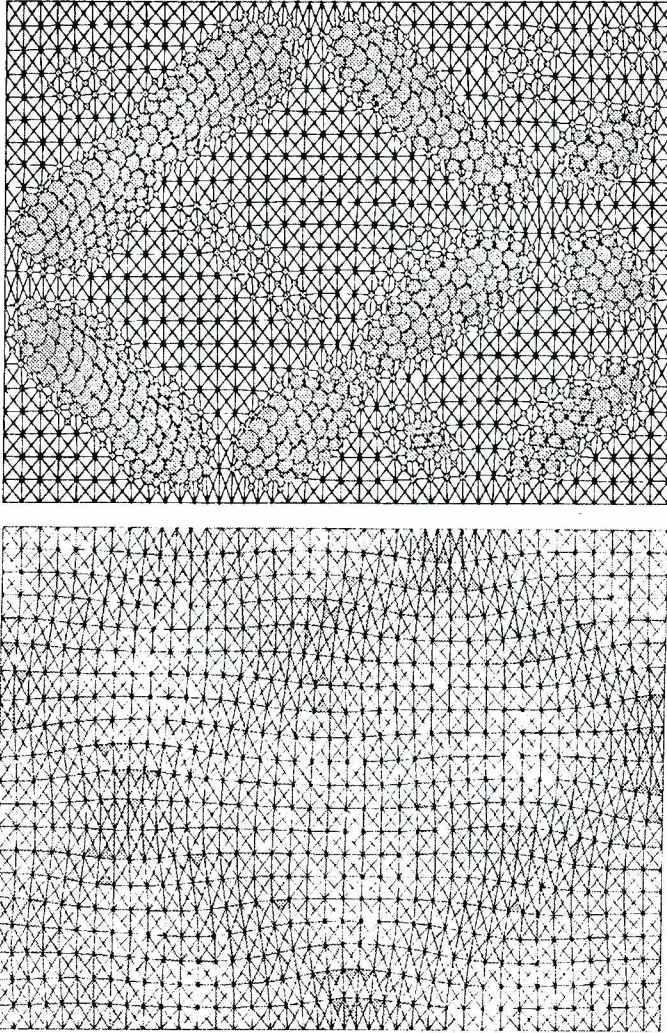
Figure 18. *Distribution of the Cosserat rotation and void ratio for dense specimen*
$(e_0 = 0.60 + 0.05r, \; d_{50} = 0.5 \; mm)$ *at residual state* $(u_1/h = 0.2)$

between the inclined zones $(s = 120 \times d_{50})$ is larger. If the uniform vertical pressure becomes greater, only one shear zone at different places is observed. The thickness of the shear zone is then about $t = 15 \times d_{50}$ (Figures 13 and 14). The shape of this zone is slightly parabolic. However, if the vertical pressure increases linearly from 0 kPa to 100 kPa, three shear zones are created with a thickness of $t = 16 \times d_{50}$ (Figure 15). The distance between the zones, $s = 50 \times d_{50}$, is significantly smaller than in Figure 4. For the medium dense specimen (Figure 16), again three shear zones appear with a thickness of $t = 20 \times d_{50}$ and a distance of $s = 60 \times d_{50}$.
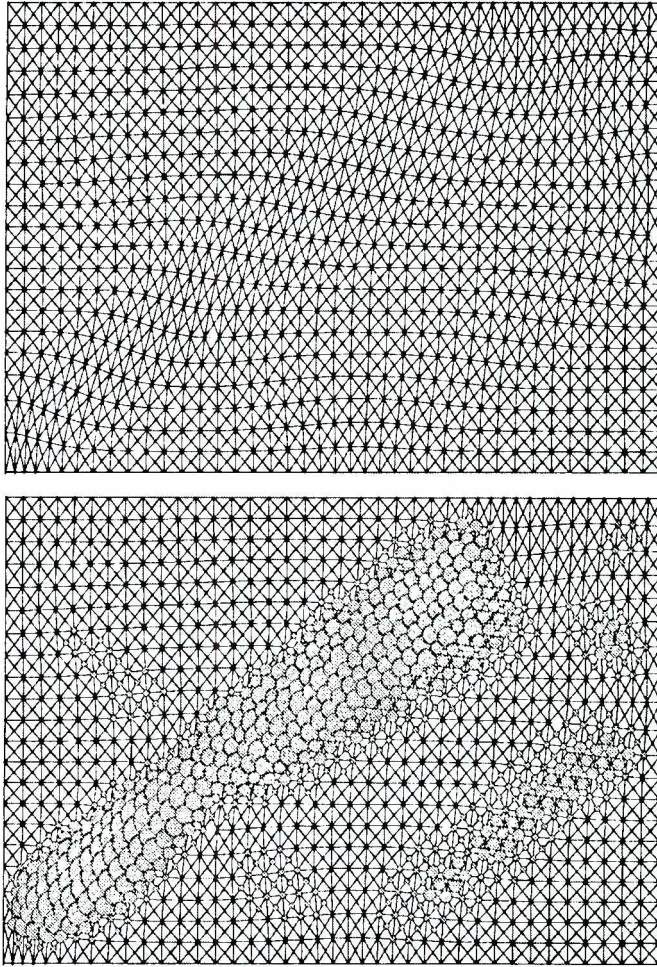
Figure 19. *Deformed mesh at residual state and the distribution of the Cosserat rotation for dense specimen ($e_0 = 0.60 + 0.05r$, $d_{50} = 0.5$ mm) at residual state ($u_1/h = 0.2$)*

The FE–calculations of a plane strain compression test with boundary conditions of Figure 3b, the K_0-initial stress state ($K_0 = 0.4$) and the stochastic distribution of the initial void ratio in the specimen are shown in Figures 17–20. The effect of the initial void ratio and its deviation was studied. The calculations show that the geometry of shear zones is strongly influenced by e_0 and a. For dense sand and a large deviation of the initial void ratio ($e_0 = 0.60 + 0.05r$), a pattern of shear zones is created (Figures 17 and 18). Their thickness and distance on the basis of the Cosserat rotation are variable. In the case of dense sand and a small deviation of the initial void ratio ($e_0 = 0.60 + 0.005r$), only one very wide shear zone occurs ($t = 30 \times d_{50}$), Figure 19. If medium dense sand with a large deviation of the initial void ratio is used ($e_0 = 0.70 + 0.05r$), one very wide shear zone also occurs with a variable thickness ($t = 25\text{-}30 \times d_{50}$), Figure 20.
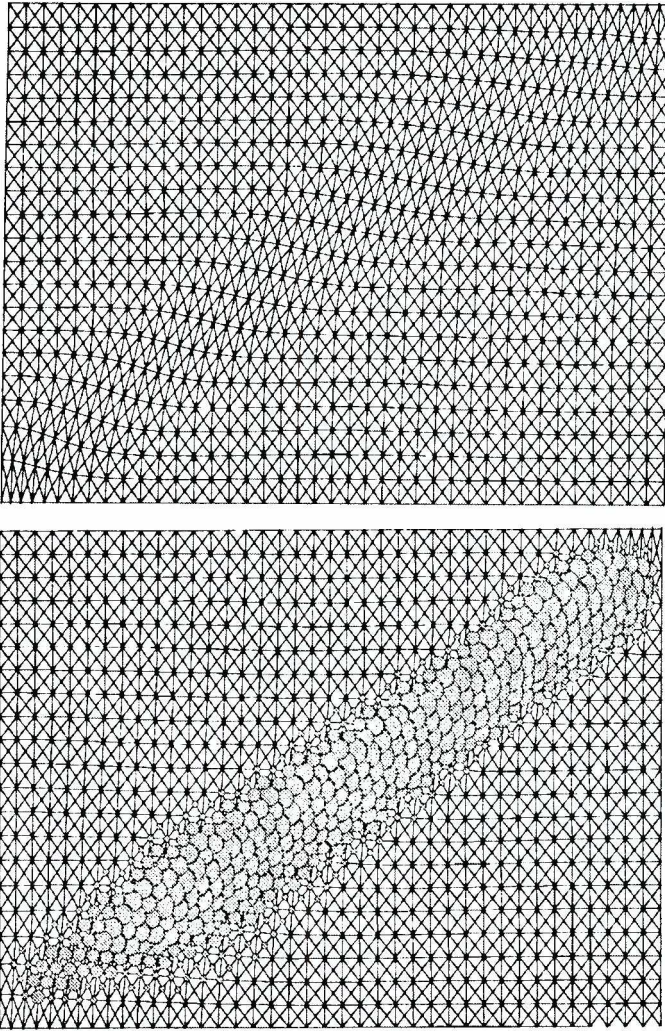
Figure 20. *Deformed mesh at residual state and the distribution of the Cosserat rotation for medium dense specimen ($e_0 = 0.70 + 0.05r$; $d_{50} = 0.5$ mm) at residual state ($u_1/h = 0.2$)*

5. Conclusions

The following conclusions can be drown on the basis of the performed FE–studies on shear localisation during plane strain compression tests:

— The shear zones have a tendency for reflection only from fixed or moving rigid boundaries.

— The geometry of shear zones depends on the conditions along the boundaries of the specimen, initial stress state and the distribution of imperfections.

— The thickness of shear zones increases with increasing initial void ratio, pressure level and mean grain diameter. If the initial void ratio approaches or exceeds the pressure-dependent critical void ratio, the shear zone reaches the size of the granular body.

— The distance between shear zones increases with decreasing initial void ratio and increasing pressure.

— The polar quantities become noticeable by shearing. The Cosserat rotation, the increasing void ratio and the non-symmetry of the stress tensor in the shear zone, and high gradients of curvatures, stresses and couple stresses at the shear zone edges can be used to identify shear zones.

The FE–calculations on the patterning of shear zones will be continued. In addition, the effect of the specimen size on the geometry of shear zones will be numerically studied.

References

[1] Bathe K. J., *Finite Element Procedures in Engineering Analysis*, Prentice-Hall, Inc., Englewood Cliffs, New Jersey, 1982

[2] Bauer E., *Calibration of a comprehensive hypoplastic model for granular materials*, Soils and Foundations **36**, 13, 1996

[3] Bauer E. and Huang W., *Numerical study of polar effects in shear zones*, Numerical Models in Geomechanics, eds. G. N. Pande, S. Pietruszczak and H. F. Schweiger, Balkema, 133, 1999

[4] Belytschko T., Chiang H. and Plaskacz E., *High resolution two dimensional shear band computations: imperfections and mesh dependence*, Com. Meth. Appl. Mech. Engng. **119**, 1, 1994

[5] Benallal A., Billardon R. and Geymonat G., *Localization phenomena at the boundaries and interfaces of solids*, Proc. of the 3rd Int. Conf. Constitutive Laws for Engineering Materials: Theory and Applications, Tucson, Arizona, eds.: C. S. Desai *et al.*, 387, 1987

[6] de Borst R., *Bifurcations in finite element models with a non-associated flow rule*, Int. J. Num. Anal. Meth. Geomech. **12**, 99, 1988

[7] de Borst R., *Simulation of strain localization: a reappraisal of the Cosserat continuum*, Engng. Computations **8**, 317, 1991

[8] de Borst R., Mühlhaus H. B., Pamin J. and Sluys L. Y., *Computational modelling of localization of deformation*, Proc. of the 3rd Int. Conf. Comp. Plasticity, eds.: D. R. J. Owen, E. Onate and E. Hinton, Pineridge Press, Swansea, 483, 1992

[9] Brinkgreve R., *Geomaterial models and numerical analysis of softening*, Dissertation, Delft University, 1, 1994

[10] Brummund W. F. and Leonards G. A., *Experimental study of static and dynamic friction between sand and typicial construction materials*, J. Test Evaluation **1**, 162, 1973

[11] Budhu M., *Non-uniformities imposed by simple shear apparatus*, Can. Geotech. J. **20**, 125, 1984

[12] Cundall P. A., *Numerical experiments on localisation in frictional materials*, Ingenieur-Archiv **59**, 148, 1989

[13] Desai C. S., Drumm E. C. and Zaman N. M., *Cyclic testing and modelling of interfaces*, J. Geotech. Engng. ASCE **111**, 793, 1985

[14] Desrues J. and Hammad W., *Shear banding dependency on mean pressure level in sand*, Int. Workshop on Numerical Methods for Localization and Bifurcation of Granular Bodies, Gdansk, Poland, 1989

[15] Desrues J., Chambon R., Mokni M. and Mazerolle F., *Void ratio evolution inside shear bands in triaxial sand specimens studied by computed tomography*, Géotechnique **46**, 529, 1996

[16] Dietsche A., *Lokale Effekte in linear-elastischen und elasto-plastischen Cosserat-Continua*, Dissertation, Karlsruhe University 1, 1993

[17] Groen A. E., *Three-dimensional elasto-plastic analysis of soils*, Dissertation, Delft University, 1997

[18] Gudehus G., *Einige Beiträge der Bodenmechanik zur Entstehung und Auswirkung von Diskontinuitäten*, Felsbau **4**, 190, 1986

[19] Gudehus G., *Localisation in granular bodies-position and objectives*, Localisation and Bifurcation Theory for Soils and Rocks, eds.: R. Chambon, J. Desrues and I. Vardoulakis, Balkema, Rotterdam, 1, 1994

[20] Gudehus G., *A comprehensive constitutive equation for granular materials*, Soils and Foundations **36**, 1, 1996

[21] Gudehus G., *Constitutive relations for granulate-liquid mixtures with a pectic constituent*, Mech. of Materials **22**, 93, 1996

[22] Gudehus G., *Attractors, percolation thresholds and phase limits of granular soils*, Powders and Grains, eds.: Behringer and Jenkins, Balkema, 169, 1997

[23] Gudehus G., *Shear localization in simple grain skeletons with polar effects*, Localisation and Bifurcation Theory for Soils and Rocks in Gifu, ed.: T. Adachi, F. Oka, A. Yashima, Balkema, 3, 1998

[24] Han C. and Vardoulakis I., *Plane strain compression experiments on water saturated fine-grained sand*, Géotechnique **41**, 49, 1991

[25] Hassan A. H., *Etude experimentale et numerique du comportement local et global dune interface sol granulaire structure*, Dissertation, Grenoble University, 1995

[26] Herle I., *Hypoplastizität und Granulometrie einfacher Korngerüste*, Publication Series of the Institute of Soil and Rock Mechanics, University Karlsruhe, 142, 1997

[27] Herle I., *A relation between parameters of a hypoplastic constitutive model and grain properties*, Localisation and Bifurcation Theory for Soils and Rocks in Gifu, eds.: T. Adachi, F. Oka, A. Yashima, Balkema, 91, 1998

[28] Herle I. and Gudehus G., *Determination of parameters of a hypoplastic constitutive model from grain properties*, Mechanics of Cohesive-Frictional Materials, 1999 (in print)

[29] Hicks M. A., *Error estimation and mesh refinement for computations of localisation in geomaterials*, Localisation and Bifurcation Theory for Soils and Rocks in Gifu, eds: T. Adachi, F. Oka, A. Yashima, Balkema, 271, 1998

[30] Hobbs B. E. and Ord A., *Numerical simulation of shear band formation in frictional-dilational material*, Ingenieur-Archiv **59**, 209, 1989

[31] Kolymbas D., *A novel constitutive law for soils*, Proc. Int. Conf. on Constitutive Laws, Tucson, ed.: C. S. Desai *et al.*, 319, 1987

[32] Lade P. V., *Localisation effects in triaxial tests on sand*, Proc. IUTAM Conference on Deformation and Failure of Granular Materials, 461, 1982

[33] Leroy Y. and Ortiz M., *Finite element analysis of strain localisation in frictional materials*, Int. J. Num. Anal. Meth. Geom. **13**, 53, 1989

[34] Loret B. and Prevost J. H., *Dynamic strain localization in fluid-saturated porous media*, ASCE J. Engng. Mech. **117**, 907, 1991

[35] Löffelmann F., *Theoretische und experimentelle Untersuchungen zur Schüttgut-Wand-Wechselwirkung und zum Mischen und Entmischen von Granulaten*, Dissertation, Karlsruhe University, 1989

[36] Murakami A. and Yoshida N., *Cosserat continuum and finite element analysis*, Deformation and Progressive Failure in Geomechanics, eds.: A. Asaoka, T. Adachi and F. Oka, Pergamon, 871, 1997

[37] Mühlhaus H. B., *Berücksichtigung von Inhomogenitäten im Gebirge im Rahmen einer Kontinuumstheorie*, Publication Series of the Institute of Soil and Rock Mechanics, University Karlsruhe **106**, 1, 1989

[38] Mühlhaus H. B., *Application of Cosserat theory in numerical solutions of limit load problems*, Ing. Arch. **59**, 124, 1989

[39] Mühlhaus H. B., *Continuum models for layered and blocky rock*, Comprehensive Rock Engineering, eds.: J. A. Hudson and Ch. Fairhurst, Pergamon Press **2**, 209, 1990

[40] Nagtegaal J. C., Parks D. M. and Rice J. R., *On numerically accurate finite element solutions in fully plastic range*, Comp. Meth. Appl. Mech. Engng. **4**, 153, 1974

[41] Nedderman R. M. and Laohakul C., *The thickness of the shear zone of flowing granular materials*, Powder Technology **25**, 91, 1980

[42] Needleman A. and Tvergaard V., *Analysis of plastic flow localisation in metals*, Appl. Mech. Rev. **45**, 3, 1992

[43] Neuffer F. and Leibnitz A., *über den Gleitwiderstand zwischen Erdstoffen und Bauwerkflächen*, Bericht aus der Bauforschung, 37, 1964

[44] Oda M., Konishi J. and Nemat-Nasser S., *Experimental micromechanical evaluation of strength of granular materials, effects of particle rolling*, Mechanics of Materials, North-Holland Publishing Comp. **1**, 269, 1982

[45] Oda M., *Micro-fabric and couple stress in shear bands of granular materials*, Powders and Grains, ed.: C. Thornton, Rotterdam, Balkema, 161, 1993

[46] Oda M., Tatsuoka F. and Yoshida T., *Void ratio in shear band of dense granular soils*, Deformation and Progressive Failure in Geomechanics, eds.: A. Asaoka, T. Adachi and F. Oka, Pergamon, 157, 1997

[47] Oda M. and Kazama H., *Micro-structure of shear band and its relation to the mechanism of dilatancy and failure of granular soils*, Géotechnique (in print)

[48] Pamin J., *Gradient-dependent plasticity in numerical simulation of localisation phenomena*, Dissertation, Delft University, 1, 1994

[49] Papanastasiou P. and Vardoulakis I., *Numerical treatment of progressive localization in relation to borehole stability*, Int. J. Num. Anal. Meth. Geomech. **16**, 389, 1992

[50] Pastor M. and Peraire J., *Capturing shear bands via adaptive remeshing techniques*, Euromech. 248: Non-linear soil-structure interaction, 1989

[51] Poliakov A., Herrmann H., Podladchikov Y. and Roux S., *Fractal plastic shear bands*, Fractals **2**, 567, 1994

[52] Potyondy J. G., *Skin friction between various soils and construction material*, Géotechnique **11**, 339, 1961

[53] Pradhan T., *Characteristics of shear band in plane strain compression test of sands*, Deformation and Progressive Failure in Geomechanics, ed. by A. Asaoka, T. Adachi and F. Oka, Pergamon, 241, 1997

[54] Ramakrshnan N. and Atluri S. N., *Simulations of shear band formations in plane strain tension and compression using FEM*, Mechanics of Materials **17**, 307, 1994

[55] Roscoe K. H., *The influence of strains in soil mechanics*, Géotechnique **20**, 129, 1970

[56] Scarpelli G. and Wood D. M., *Experimental observations of shaer band patterns in direct shaer tests*, Proc. IUTAM Conference on Deformation and Failure of Granular Materials, 473, 1982

[57] Schanz T., Desrues J. and Vermeer P. A., *Comparison of sand data on different plane strain devices*, Deformation and Progressive Failure in Geomechanics, A. Asaoka, T. Adachi and F. Oka, Pergamon, 289, 1997

[58] Schäfer H., *Versuch einer Elastizitätstheorie des zweidimensionalen ebenen Cosserat-Kontinuums*, Miszellaneen der Angewandten Mechanik, Festschrift Tolmien, W., Berlin, Akademie-Verlag, 1962

[59] Shuttle D. A. and Smith I. M., *Numerical simulation of shear band formation in soils*, Int. J. Num. And Anal. Meth. In Geomech. **12**, 611, 1988

[60] Schwing E., *Standsicherheit historischer Stützwände*, Publication Series of the Institute of Soil and Rock Mechanics, University Karlsruhe **121**, 1, 1991

[61] Sluys L. J., *Wave propagation, localisation and dispersion in softening solids*, Dissertation, Delft University of Technology, 1992

[62] Sondermann W., *Spannungen und Verformungen bei bewehrter Erde*, Mitteilungen des Instituts für Grundbau, Universität Braunschweig, 1983

[63] Stazhevskii S. B. and Revushenko A. F., *Lokalisation in granular materials*, Lecture at the Karlsruhe University, Germany, 1992

[64] Steinmann P., *Theory and numerics of ductile micropolar elastoplastic damage*, Int. J. for Num. Meth. in Engng. **38**, 583, 1995

[65] Tatsuoka F., Siddiquee M. S., Yoshida T., Park C. S., Kamegai Y., Goto S., Kohata S. and Y., *Testing methods and results of element tests and testing conditions of plane strain model bearing capacity tests using air-dried dense Silver Buzzard Sand*, Internal Report, University of Tokyo, 1, 1994

[66] Tatsuoka F., Okahara M., Tanaka T., Tani K., Morimoto T. and Siddiquee M. S., *Progressive failure and particle size effect in bearing capacity of footing on sand*, Proc. of the ASCE Geotechnical Engineering Congress **27**, 788, 1991

[67] Tatsuoka F., Goto S., Tanaka T., Tani K. and Kimura Y., *Particle size effects on bearing capacity of footing on granular material*, Deformation and Progressive Failure in Geomechanics, eds.: Asaoka, A., Adachi, T. and Oka, F. Pergamon, 133, 1997

[68] Tejchman J., *Scherzonenbildung und Verspannungseffekte in Granulaten unter Berücksichtigung von Korndrehungen*, Publication Series of the Institute of Soil and Rock Mechanics, University Karlsruhe **117**, 1, 1989

[69] Tejchman J. and Wu W., *Numerical study on shear band patterning in a Cosserat continuum*, Acta Mech. **99**, 61, 1993

[70] Tejchman J. and Gudehus G., *Silo-music and silo-quake, experiments and a numerical Cosserat approach*, Powder Technology **76**, 201, 1993

[71] Tejchman J., *Numerical study on localised deformation in a Cosserat continuum, Localisation and Bifurcation Theory for Soils and Rocks*, eds.: R. Chambon, J. Desrues and I. Vardoulakis, Balkema, Rotterdam, 257, 1994

[72] Tejchman J., *Grain size effects in bearing capacity of a strip foundation*, Numerical Models in Geomechanics, NUMOG, Davos, ed.: G. N. Pande and S. Pietruszczak, 571, 1995

[73] Tejchman J. and Wu W., *Experimental and Numerical Study of Sand-Steel Interfaces*, Int. J. Num. Anal. Meth. Geomech. **19**, 513, 1995

[74] Tejchman J. and Bauer E., *Numerical simulation of shear band formation with a polar hypoplastic model*, Computers and Geotechnics **19**, 221, 1996

[75] Tejchman J. and Wu W., *Dynamic patterning of shear bands in a Cosserat continuum*, International Journal of Engineering Mechanics ASCE **123**, 123, 1997

[76] Tejchman J., *Modelling of shear localisation and autogeneous dynamic effects in granular bodies*, Publication Series of the Institute of Soil and Rock Mechanics, University Karlsruhe **140**, 1, 1997

[77] Tejchman J., *Modelling of shear localisation with a polar hypoplastic approach*, Localisation and Bifurcation Theory for Soils and Rocks in Gifu, eds.: T. Adachi, F. Oka, A. Yashima, Balkema, 323, 1998

[78] Tejchman J., Herle I. and Wehr J., *FE–studies on the influence of initial void ratio, pressure level and mean grain diameter on shear localisation*, Int. J. Num. Anal. Meth. Geomech. **23**, 2045, 1999

[79] Tejchman J. and Herle I., *A class A prediction of the bearing capacity of plane strain footings on granular material*, Soils and Foundations **39**, 47, 1999

[80] Tejchman J., *Behaviour of granular bodies in induced shear zones*, Granular Matters **2**, 77, 2000

[81] Tejchman J. and Ummenhofer T., *Bedding effects in bulk solids in silos — experiments and a polar hypoplastic approach*, Thin-Walled Structures **4**, 2000 (in print)

[82] Uesugi M., Kishida H. and Tsubakihara Y., *Behaviour of sand particles in sand-steel friction*, Soils and Foundations **28**, 107, 1988

[83] Unterreiner P., Vardoulakis I., Boulon M. and Salem J., *Essential features of a Cosserat continuum in interfacial localisation*, Localisation and Bifurcation Theory for Soils and Rocks, eds.: R. Chambon, J. Desrues and I. Vardoulakis, Balkema, 141, 1994

[84] Vardoulakis I., *Shear band inclination and shear modulus in biaxial tests*, Int. J. Num. Anal. Meth. Geomech. **4**, 103, 1980

[85] Vardoulakis I., Graf B. and Gudehus G., *Trap-door problem with dry sand: a statical approach based upon model test kinematics*, International Journal for Numerical and Analytical Methods in Geomechanics **5**, 57, 1981

[86] Wehr J., Tejchman J., Herle I. and Gudehus G., *Sand anchors — a shear zone problem*, Deformation and Progressive Failure in Geomechanics, eds.: A. Asaoka, T. Adachi and F. Oka, Pergamon, 787, 1997

[87] Wehr J. and Tejchman J., *Sand anchors in rock and granular soils — experiments and a polar hypoplastic approach*, Proc. World Civil and Environmental Engineering Conference, Thailand, 8–12 XI 1999, ed. A.S. Balasubramaniam *et al.* **2**, VII 1, 1999

[88] Vermeer P. A. and van Langen H., *Soil collapse computations with finite elements*, Ing. Arch. **59**, 221, 1989

[89] Wernick E., *Tragfähigkeit zylindrischer anker in sand unter besonderer Berücksichtigung des Dilatanzverhaltens*, Publication Series of the Institute of Soil and Rock Mechanics, University Karlsruhe **75**, 1, 1978

[90] von Wolffersdorff P. A., *A hypoplastic relation for granular materials with a predefined limit state surface*, Mechanics of Cohesive-Frictional Materials **1**, 251, 1996

[91] Wu W., Bauer E. and Kolymbas D., *Hypoplastic constitutive model with critical state for granular materials*, Mechanics of Materials **23**, 45, 1996

[92] Wu W. and Niemunis A., *Failure criterion, flow rule and dissipation function derived from hypoplasticity*, Mechanics of Cohesive-Frictional Materials **1**, 145, 1996

[93] Yagi K., Miura S., Asonuma T., Sakon T. and Nakata T., *Particle crushing and shear banding of volcanic coarse-grained soils*, Deformation and Progressive Failure in Geomechanics, eds.: A. Asaoka, T. Adachi and F. Oka, Pergamon, 139, 1997

[94] Yoshida T., Tatsuoka F. and Siddiquee M., *Shear banding in sands observed in plane strain compression*, Localisation and Bifurcation Theory for Soils and Rocks, eds.: R. Chambon, J. Desrues and I. Vardoulakis, Balkema, Rotterdam, 165, 1994

[95] Yoshida N., Arai T. and Onishi K., *Elasto-plastic Cosserat finite element analysis of ground deformation under footing load*, Deformation and Progressive Failure in Geomechanics, eds.: A. Asaoka, T. Adachi and F. Oka, Pergamon, 395, 1997

[96] Yoshimi Y. and Kishida T., *Friction between sand and metal surface*, Proc. of the 10th ICSMFE **1**, 831, 1981